Celest Mech Dyn Astr (2010) 106:117–142
DOI 10.1007/s10569-009-9246-x

ORIGINAL ARTICLE

Using space manifold dynamics to deploy a small satellite constellation around the Moon

Riccardo Marson · Mauro Pontani · Ettore Perozzi · Paolo Teofilatto

Received: 19 November 2008 / Revised: 23 November 2009 / Accepted: 25 November 2009 /
Published online: 30 December 2009

Abstract The possibility of communicating with the far side of the Moon is essential for keeping a continuous radio link with lunar orbiting spacecraft, as well as with manned or unmanned surface facilities in locations characterized by poor coverage from Earth. If the exploration and the exploitation of the Moon must be sustainable in the medium/long term, we need to develop the capability to realize and service such facilities at an affordable cost. Minimizing the spacecraft mass and the number of launches is a driving parameter to this end. The aim of this study is to show how Space Manifold Dynamics can be profitably applied in order to launch three small spacecraft onboard the same launch vehicle and send them to different orbits around the Moon with no significant difference in the Delta-V budgets. Internal manifold transfers are considered to minimize also the transfer time. The approach used is the following: we used the linearized solution of the equations of motion in the Circular Restricted Three Body Problem to determine a first–guess state vector associated with the Weak Stability Boundary regions, either around the collinear Lagrangian point L1 or around the Moon. The resulting vector is then used as initial state in a numerical backward-integration sequence that outputs a trajectory on a manifold. The dynamical model used in the numerical integration is four-body and non-circular, i.e. the perturbations of the Sun and the lunar orbital eccentricity are accounted for. The trajectory found in this way is used as the principal segment of the lunar transfer. After separation, with minor maneuvers each satellite

R. Marson (✉) · E. Perozzi
Telespazio S.p.A., Rome, Italy
e-mail: guest468.marson@telespazio.com

M. Pontani · P. Teofilatto
Università di Roma, "La Sapienza", Rome, Italy
e-mail: mauro.pontani@uniroma1.it

P. Teofilatto
e-mail: paolo.teofilatto@uniroma1.it

E. Perozzi
Space Academy Foundation, Rome, Italy
e-mail: ettore.perozzi@telespazio.com

is injected into different orbits that lead to ballistic capture around the Moon. Finally, one or more circularization maneuvers are needed in order to achieve the final circular orbits. The whole mission profile, from launch to insertion into the final lunar orbits, is modeled numerically with the commercial software STK.

Keywords Space manifold dynamics · Lunar exploration · Weak stability boundary · Low energy transit orbits

Abbreviations

CR3BP	Circular restricted three body problem
DU	Distance unit
EL1	Earth–Sun Lagrange point 1
EL2	Earth–Sun Lagrange point 2
EIRP	Effective isotropic radiated power
LL1	Lunar Lagrange point 1
LL2	Lunar Lagrange point 2
SMD	Space manifold dynamics
STK	Satellite tool kit
WSB	Weak stability boundary
ZVS	Zero velocity surface

1 Introduction

In the past few years there has been a renewed interest in the exploration of the Moon, and the future plans of the major space agencies foresee the realization of lunar missions. It is also becoming clear that the exploration of the far side of the Moon will play a significant role in this scenario. In 2005 NASA issued an Exploration Systems and Architecture Study (NASA 2005) that defined ten high-priority lunar landing sites where the very first missions should be focused. It is interesting to note that four out of ten of these sites are located on the far side, two at the poles and the remaining four on the near side. Since direct communication with the Earth from the far side of the Moon is not possible, it becomes necessary to develop facilities that will enable future unmanned vehicles and crews to keep a constant link with mission control. In addition, servicing missions must be as low-cost as possible in order to make the exploration of the Moon sustainable over a long period of time. The total cost of a mission will not only depend upon the total Delta-V necessary for the spacecraft to reach its intended orbit, but also upon the cost of the spacecraft itself. Key parameters are the propulsion system (whether chemical or electrical), and the mission lifetime (i.e. the fuel needed for station keeping). When more than one spacecraft is involved in a single mission or in maintaining a space infrastructure, another key parameter is the number of launches needed to put all the spacecraft in place and/or to service such infrastructure.

Thus, in the present study, aside from minimizing the total Delta-V, we will try to reduce as much as possible the fraction of the Delta-V that must be delivered by the spacecraft and to allow simultaneous launch of multiple spacecrafts. To do this, it would be desirable: (1) to be able to change significantly the spacecraft trajectories with little fuel expense (e.g. using electrical engines) and (2) perform ballistic capture into lunar orbit (i.e. no insertion burn). Both requirements are satisfied by low-energy non-keplerian orbits known as "Weak Stability Boundary" (WSB) transfers (Conley 1968; Gomez et al. 2004; Belbruno 2004). WSB trajectories are usually split into two groups, named "Internal" and "External"

transfers. In the Earth–Moon system, the former represent trajectories approaching the Moon from the region around the interior equilibrium point L1, while the latter represents trajectories encountering the Moon from the exterior equilibrium point L2 (Circi and Teofilatto 2006). Only Internal WSB transfers in the Earth–Moon system will be investigated in the present work.

WSB transfers have been recently considered within the framework of the treatment of trajectories lying on a manifold-shaped surface, which represent special solutions of the Circular Restricted Three Body Problem (CR3BP). It has been therefore proposed (Perozzi and Ferraz-Mello 2009; Garcia and Gomez 2007) to refer to all the applications to mission design sharing this common dynamical ground as "Space Manifold Dynamics" (SMD).

SMD is today a very active research field with a considerable number of papers published on the subject in recent years, covering various aspects of the problem (Leiva and Briozzo 2008; Érdi et al. 2009; Baig and McInnes 2009; Mingotti et al. 2009; Barrabés et al. 2009; Pergola et al. 2009, just to name a few).

The aim of this study is to show how Space Manifold Dynamics can be profitably applied in order to launch three small spacecraft onboard the same launcher and send them to different orbits around the Moon with no significant difference in the Delta-V budget. Furthermore, it will be shown that most of this budget is charged to the launcher and that the spacecraft masses can be kept reasonably small. It will also be shown how target conditions can be computed using a linearized model and transported with a fair degree of accuracy to a nonlinear model. Propagation of the whole mission profile in the elliptical three-body problem is done with STK.

In Sect. 2, the theory of the CR3BP will be briefly outlined, along with a detailed description of the types of orbit in the L1 region and their properties. In the following sections, two different strategies used to compute numerically Internal WSB transfers will be outlined, along with some examples. In particular, Sect. 3 deals with trajectories computed by targeting a Lyapunov or quasi-periodic orbit around L1 and then finding a suitable asymptotic orbit associated to it. Section 4 addresses trajectories computed by targeting the WSB region associated with certain arrival conditions at the Moon. In the fifth and final section the results of Sects. 3 and 4 will be applied to studying the launch and deployment of a three-satellite constellation around the Moon.

2 Classification of orbits around L1

The equations of motion of a spacecraft in the Earth–Moon gravitational field are usually written in a rotating frame with origin in the mass center of the Earth–Moon system. The angular rate ω is equal to the orbital angular velocity of the system composed of the two celestial bodies (termed the primaries). The distance unit (DU) is the Earth–Moon distance, whereas the time unit is such that the period of the two primaries equals 2π. Under these assumptions, the vector $\vec{x} = (x, y, z)$ denotes the position vector, whereas $\vec{V} = (u, v, w)$ represents the velocity vector (i.e. it includes the derivatives of the coordinates $\vec{x} = (x, y, z)$ with respect to the dimensionless time $\tau = \omega t$). With these settings the Earth is placed along the horizontal axis x in the position $-\mu$ and the Moon is placed along the same axis in the position $1 - \mu$, where μ represents the Moon gravitational constant in the Earth–Moon system. Then the equations of motion are:

$$\begin{cases} \frac{dx}{d\tau} = u \\ \frac{dy}{d\tau} = v \\ \frac{dz}{d\tau} = w \\ \frac{du}{d\tau} = \Omega_x + 2v \\ \frac{dv}{d\tau} = \Omega_y - 2u \\ \frac{dw}{d\tau} = \Omega_z \end{cases} \tag{1}$$

where the potential function Ω is defined as: $\Omega = \frac{1}{2}(x^2 + y^2) + \frac{1-\mu}{r_1} + \frac{\mu}{r_2}$.

Equations (1) admit the Jacobi integral (Moeckel 2005)

$$H(\vec{x}, \vec{V}) = \frac{1}{2}(u^2 + v^2 + w^2) - \Omega(x, y, z) = \frac{1}{2}\vec{V} \cdot \vec{V} - \Omega$$

For any positive constant value λ, the integral manifold is defined as

$$M(\lambda) = \left\{ \left(\vec{x}, \vec{V}\right) \in \Re^6 s.t. H\left(\vec{x}, \vec{V}\right) = -\lambda \right\}$$

which is a five-dimensional manifold in the six-dimensional state space $\left(\vec{x}, \vec{V}\right)$.

The projection of the integral manifold along the position coordinates is a volume referred to as *Hill's region*

$$S(\lambda) = \left\{ \vec{x} \in \Re^3 s.t. \exists \vec{V} : H\left(\vec{x}, \vec{V}\right) = -\lambda \right\}$$

The boundary of the Hill's region is represented by the Zero Velocity Surface (ZVS)

$$\Omega(x, y, z) = \lambda$$

In terms of the more usual Jacobi constant C (Szebehely 1967):

$$C = 2\Omega(\vec{x}) - \vec{V} \cdot \vec{V}$$

the ZVS is defined as

$$\Omega(x, y, z) = \frac{C}{2}$$

Figure 1 shows the ZVS corresponding to three distinct values of the Jacobi constant C. In Fig. 1a the motion is allowed either inside the ovals surrounding the Earth and the Moon or outside the surface enveloping both the celestial bodies. Figure 1b illustrates the case corresponding to a lower value of C, allowing internal transfers through the intermediate Lagrange point L1. Lastly, Fig. 1c portrays the zero velocity surfaces associated with a value of C that permits also external transfers to the Moon through the collinear point L2.

The integral manifold $M(\lambda)$ is the product of the three-dimensional Hill's region $\mathbb{S}(\lambda)$ and the velocity locus defined by

$$\rho^2 = (u^2 + v^2 + w^2) = 2(\Omega(x, y, z) - \lambda) \tag{2}$$

From Eq. (2) it is apparent that the velocity locus is a sphere S^2_ρ of variable radius ρ. The radius ρ tends to zero as the point (x, y, z) tends to the ZVS. In more technical terms the integral manifold is then a S^2 fiber bundle over the Hill's region:

$$\begin{aligned} &\pi : M(\lambda) \to \mathbb{S}(\lambda), \quad \pi^{-1}(\vec{x}) = S^2_\rho \\ &(\vec{x}, \vec{V}) \to \vec{x} \end{aligned}$$

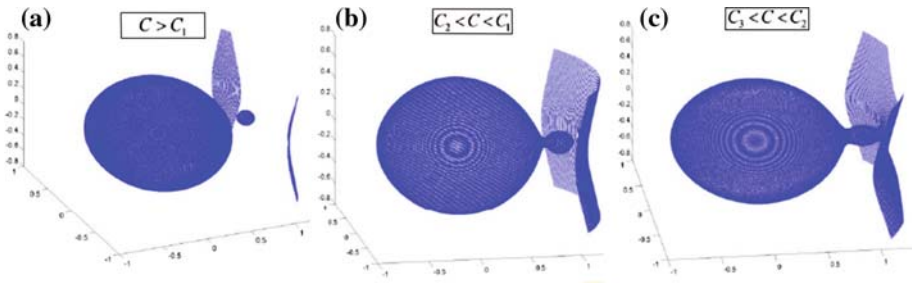

Fig. 1 The zero velocity surfaces corresponding to the following Jacobi constants C: **a** ±35.13, **b** ±35.13, **c** ±35.13, where ±35.13 is the Jacobi constant related to the Lagrangian collinear equilibrium points ±35.13, ±35.13

Low energy transit orbits from Earth to Moon are trajectories passing through the neck of the Hill' region sited about the Lagrangian collinear equilibrium point L_1 of the Earth–Moon system (cf. Fig. 1b). This result emerges from numerical simulations and is consistent with the original work made by Conley (1968).

In (Conley 1968) a classification of the orbits around Lagrangian collinear equilibrium points is given in the context of the planar restricted three-body problem. Using analytical arguments similar to those developed in (Conley 1968), such a classification is here generalized to the spatial restricted three body problem with application to the intermediate Lagrangian point L_1 of the Earth–Moon system.

The above Eq. (1) are linearized around L_1: the reference frame is centered in the Lagrangian point $L_1 = (x_{L_1}, 0, 0)$, so the new position coordinates (ξ, η, ζ) are : $\xi = x - x_{L_1}$, $\eta = y$, $\zeta = z$ and the linear equations of motion are:

$$\begin{bmatrix} \dot{\xi} \\ \dot{\eta} \\ \dot{\zeta} \\ \dot{u} \\ \dot{v} \\ \dot{w} \end{bmatrix} = \begin{bmatrix} 0 & 0 & 0 & 1 & 0 & 0 \\ 0 & 0 & 0 & 0 & 1 & 0 \\ 0 & 0 & 0 & 0 & 0 & 1 \\ a & 0 & 0 & 0 & 2 & 0 \\ 0 & -b & 0 & -2 & 0 & 0 \\ 0 & 0 & -c & 0 & 0 & 0 \end{bmatrix} \begin{bmatrix} \xi \\ \eta \\ \zeta \\ u \\ v \\ w \end{bmatrix} \tag{3}$$

where $a = 1 + 2\gamma^2, b = \gamma^2 - 1, c = \gamma^2$ and $\gamma^2 = \frac{1-\mu}{|x_{L_i}+\mu|^3} + \frac{\mu}{|x_{L_i}+\mu-1|^3}$.

The eigenvalues of the matrix of the linear system are:

$$\lambda_1 = \alpha, \quad \lambda_2 = -\alpha, \quad \lambda_3 = i\omega_{xy}, \quad \lambda_4 = -i\omega_{xy}, \quad \lambda_5 = i\omega_z, \quad \lambda_4 = -i\omega_z$$

where $\alpha = \sqrt{s_+}, \omega_{xy} = \sqrt{s_-}, \omega_z = \gamma, s_\pm = \frac{\gamma^2-2}{2} \pm \frac{\sqrt{9\gamma^4-8\gamma^2}}{2}$. The eigenvectors are

$$\vec{v}_1 = \begin{bmatrix} 1 \\ \sigma \\ \alpha \\ \alpha\sigma \\ 0 \\ 0 \end{bmatrix}, \vec{v}_2 = \begin{bmatrix} 1 \\ -\sigma \\ -\alpha \\ \alpha\sigma \\ 0 \\ 0 \end{bmatrix}, \vec{v}_3 = \begin{bmatrix} 1 \\ i\tau \\ i\omega_{xy} \\ -\omega_{xy}\tau \\ 0 \\ 0 \end{bmatrix}, \vec{v}_4 = \begin{bmatrix} 1 \\ -i\tau \\ -i\omega_{xy} \\ -\omega_{xy}\tau \\ 0 \\ 0 \end{bmatrix}, \vec{v}_5 = \begin{bmatrix} 0 \\ 0 \\ 0 \\ 0 \\ 1 \\ i\omega_z \end{bmatrix},$$

$$\vec{v}_6 = \begin{bmatrix} 0 \\ 0 \\ 0 \\ 0 \\ 1 \\ -i\omega_z \end{bmatrix}$$

where

$$\sigma = \frac{-2\alpha}{\alpha^2 + \gamma^2 - 1}, \quad \tau = \frac{-2\omega_{xy}}{\gamma^2 - 1 - \omega_{xy}^2}, \quad \gamma^2 = \frac{1-\mu}{|x_{L_i} + \mu|^3} + \frac{\mu}{|x_{L_i} + \mu - 1|^3}$$

Note that the eigenvectors depend on the eigenvalues $(\alpha, \omega_{xy}, \omega_z)$ and on the above constants (σ, τ).

Then the general solution $\vec{U}(t)$ of the linearized motion around L_1 takes the form:

$$\vec{U}(t) = \alpha_1 e^{\alpha t}\vec{v}_1 + \alpha_2 e^{-\alpha t}\vec{v}_2 + \mathrm{Re}\left(A_{xy}e^{i\omega_{xy}t+\phi_{xy}}\vec{v}_3\right) + \mathrm{Re}\left(A_z e^{i\omega_{zy}t+\phi_z}\vec{v}_4\right) \tag{4}$$

This motion is the sum of two divergent terms, proportional to α_1 and α_2, and a quasi-periodic motion characterized by the two (non-commensurable) frequencies ω_{xy} and ω_z and by the two amplitudes A_{xy} and A_z. The constant parameters $\alpha_1, \alpha_2, A_{xy}, A_z, \phi_{xy}, \phi_z$ depend on the initial conditions $(\xi_0, \eta_0, \zeta_0, u_0, v_0, w_0)$.

Equation (4) allows an immediate classification for the orbits:

(1) Quasi-periodic orbits: these are the solutions with $\alpha_1 = \alpha_2 = 0$
(2) Asymptotic orbits: these are the orbits with $\alpha_1 = 0, \alpha_2 \neq 0$ (orbits approaching the quasi-periodic orbit), or $\alpha_1 \neq 0, \alpha_2 = 0$ (orbits generated from the quasi-periodic orbit).
(3) Transit orbits: these are the solutions with $\alpha_1\alpha_2 < 0$. For instance, orbits with $\alpha_1 > 0$ and $\alpha_2 < 0$ cross the L_1 region from left to right (from the Earth to the Moon).
(4) Bouncing orbits: these are the solutions with $\alpha_1\alpha_2 > 0$. For instance, orbits with $\alpha_1 > 0$ and $\alpha_2 > 0$approach the L_1 region departing from the Earth, and come back to the Earth without crossing the L_1 region.

Transfer orbits from Earth to Moon are (in the linear sense) transit orbits with $\alpha_1 > 0$ and the locus of these orbits will be determined in the phase space according to the linear equations of motion (3). However, the following questions arise: can this locus be defined when the nonlinear flow is considered? Which are the properties of these orbits in terms of the initial orbital elements (with respect to the Earth) and the final orbital elements (with respect to the Moon)? These issues can be addressed as follows: first, let $\vec{x}_0 = (\xi_0, \eta_0, \zeta_0, u_0, v_0, w_0)$ be a point belonging to the locus of transit orbits (and close to L_1). Then, the states at periselenium and at perigee are obtained by forward and backward propagation of $\vec{x}_0$, using the nonlinear equations (1). What will be shown is that lower altitude perigees and periselenia correspond to initial conditions (for propagation) $\vec{x}_0$ close to those yielding asymptotic orbits when the linear model is assumed.

2.1 Asymptotic orbits: characterization of position

Let us determine the locus of orbits that are asymptotic with respect to the linear equations (3). The linearized equations of motion admit the energy integral

$$h = \frac{1}{2}(\upsilon^2 + v^2 + w^2) - \frac{a}{2}\xi^2 + \frac{b}{2}\eta^2 + \frac{c}{2}\varsigma^2 \tag{5}$$

The integral h can be written as a quadratic form:

$$h = \frac{1}{2}\vec{U}\mathrm{G}\vec{U} \tag{6}$$

with

$$\mathrm{G} = \begin{bmatrix} \mathrm{E}\ 0_{4\times 2} \\ 0_{2\times 4}\mathrm{F} \end{bmatrix}, \quad E = \begin{bmatrix} -a & & & \\ & b & & \\ & & c & \\ & & & 1 \end{bmatrix}, \quad F = \begin{bmatrix} 1 & \\ & 1 \end{bmatrix}$$

and $\vec{U} = (\xi, \eta, \zeta, u, v.w)$ is the solution of the linear equations of motion.

On the other hand, using the expression (4) for $\vec{U}$, one obtains:

$$h = \alpha_1\alpha_2 e_1 + A_{xy}^2 e_2 + A_z^2 e_3 \tag{7}$$

where

$$e_1 = \vec{v}_1 E \vec{v}_2, \quad e_2 = \vec{v}_3 E \vec{v}_4, \quad e_3 = \vec{v}_5 E \vec{v}_6 \tag{8}$$

According to Eq. (7), the asymptotic orbits have the following energy:

$$h = A_{xy}^2 \quad e_2 + A_z^2 \quad e_3 \tag{9}$$

With reference to the same analytic arguments of (Conley 1968), a point (ξ, η, ς) can generate an asymptotic orbit of energy h if the following conditions are satisfied:

$$-\frac{a}{2}\xi^2 + \frac{b}{2}\eta^2 + \frac{c}{2}\zeta^2 \leq h \tag{10}$$

and

$$\eta = -\sigma\xi \pm 2A_{xy}(\sigma^2 + \tau^2) \leftrightarrow \text{orbits departing from the Earth side } (\alpha_1 = 0) \tag{11}$$

or

$$\eta = \sigma\xi \pm 2A_{xy}(\sigma^2 + \tau^2) \leftrightarrow \text{orbits departing from the Moon side } (\alpha_2 = 0) \tag{12}$$

For a given energy h, the above conditions imply that the points which generate asymptotic orbits project within one of the two stripes (11), (12), lying on the (ξ, η) plane. The third coordinate ζ is such that the associated point belongs to the Hill's region of energy h. Hence, the asymptotic orbits are located within the corridor whose walls depart from the boundaries of the stripes (11) and (12) and end at the zero velocity surface, which can be viewed as the "ceiling" (Fig. 2). In fact the width of the corridor depends on the out-of-plane amplitude A_z. Namely, if h is fixed to a specific value, the in-plane amplitude of the asymptotic orbit is equal to (cf. Eq. (9)):

$$A_{xy} = \left(\frac{h - A_z^2 e_3}{e_2}\right)^{\frac{1}{2}} \tag{13}$$

and the out-of-plane amplitude is constrained to:

$$0 \leq A_z < \sqrt{\frac{h}{e_3}} \tag{14}$$

Of course higher values of the out-of-plane amplitude reduce the amplitude of the in-plane periodic motion as well as the width of the strip of the asymptotic solutions.

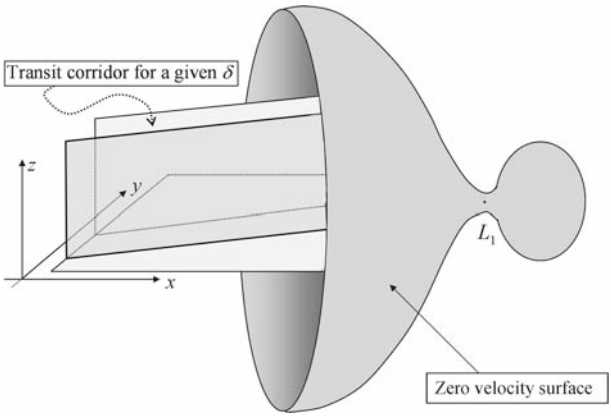

Fig. 2 The corridor where asymptotic orbits are located

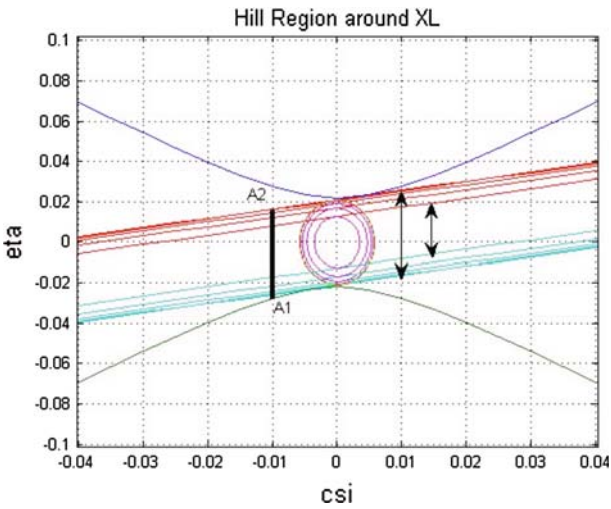

Fig. 3 Plot of the (ξ, η) region around L1. The strip of the ± 35.13 asymptotic orbits for $h = 0.001$ and for four different values of the out-of-plane amplitude ± 35.13 are shown. The *up down arrows* show the width of the ± 35.13 case (maximum width) and the width of the ± 35.13 case (minimum width)

For instance, if the value μ of the Moon is set to $\mu = 0.01214$ and the energy value to $h = 0.001$, one obtains

$$0 \leq A_z < 0.00985$$

Figure 3 shows the planar projection of the boundary of the Hill's region corresponding to $h = 0.001$, the projection of the quasi-periodic orbit and four stripes associated to the $(\alpha_1 = 0)$-asymptotic orbits. These stripes correspond to the following four different values of A_z:

$$A_z = 0, \quad A_z = 0.00197, \quad A_z = 0.00394, \quad A_z = 0.00591$$

It is apparent that the width of the strip of the asymptotic orbits decreases as the out-of-plane amplitude increases.

2.2 Asymptotic orbits: characterization of velocity

The initial position must lie on the above defined corridor in order to obtain an asymptotic orbit. However, also some conditions on the initial velocity must be satisfied. Consider any point $(\xi_0, \eta_0, \varsigma_0)$ within the corridor of asymptotic orbits associated with $\alpha_1 = 0$. In particular the coordinates ξ_0 and ζ_0 are assumed as specified and the coordinate η_0 is selected along a vertical segment, as shown in Fig. 3 (where $\xi_0 = -0.01$). Each point $(\xi_0, \eta_0, \varsigma_0)$ is associated to a value ρ of the velocity magnitude:

$$\rho^2 = 2h + a\xi_0^2 - b\eta_0^2 - c\varsigma_0^2 \tag{15}$$

Hence, the tip of the velocity vector corresponding to $(\xi_0, \eta_0, \varsigma_0)$ belongs to a sphere of variable radius; let δ and θ be the polar and azimuth angles of the direction of the velocity $\vec{V} = (u, v, w)$:

$$\begin{aligned} u &= \rho\ \cos\delta\ \cos\theta \\ v &= \rho\ \cos\delta\ \sin\theta \\ w &= \rho\ \sin\delta \end{aligned} \tag{16}$$

In the following, the condition $\alpha_1 = 0$, as well as the sign of the coefficient α_1, will be related to the angles (θ, δ).

Note that any point η_0 taken along the vertical segment is inside the strip related to $A_z = 0$. If the value of A_z increases, the width of the strip of asymptotic orbits decreases and the point η_0 could exit the strip. The maximum allowed value for A_z is the value corresponding to the strip with boundary passing through the point (ξ_0, η_0) (cf. Eqs. (12), (13)):

$$A_z^{\max} = \left| \frac{1}{e_3} \left(h - \frac{e_2}{4} \frac{(\eta_0 - \sigma\xi_0)^2}{(\sigma^2 + \tau^2)^2} \right) \right|^{\frac{1}{2}} \tag{17}$$

On the other hand, A_z is related to the out-of-plane initial conditions

$$A_z = \left\{ \frac{1}{2} \left(z_0^2 + \frac{w_0^2}{\omega_z^2} \right) \right\}^{\frac{1}{2}}. \tag{18}$$

$A_z^{\max}$ is associated to the maximum (and minimum) allowed value of the angle δ through the relationships (18) and (16), which yield:

$$\delta_{\max} = \left| a \sin \left[\frac{\omega_z}{\rho} (2A_z^{\max^2} - \zeta_0^2) \right] \right|, \quad \delta_{\min} = -\delta_{\max} \tag{19}$$

If $\alpha_1 = 0$ (asymptotic solutions), then the angle θ, introduced in (16), turns out to be equal to one of the following two values:

$$\begin{cases} \theta = \theta_{\min} = \chi_1 - a\cos\left(\frac{\kappa_1}{\cos\delta}\right) \\ \theta = \theta_{\max} = \chi_1 + a\cos\left(\frac{\kappa_1}{\cos\delta}\right) \end{cases} \tag{20}$$

where

$$\kappa_1 = -\frac{a\xi_0 + b\sigma\eta_0}{\alpha\rho(1+\sigma^2)^{\frac{1}{2}}}$$

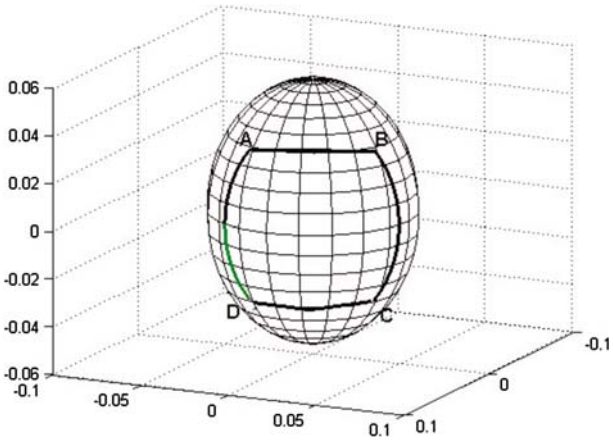

Fig. 4 Velocity locus: the region of transit-asymptotic orbits

and χ_1 is the angle between the ξ coordinate axis and the straight line $\eta = -\sigma\xi$; as a consequence, χ_1 is defined by

$$\cos\chi_1 = \sqrt{\frac{1}{1+\sigma^2}}, \quad \sin\chi_1 = \sqrt{\frac{-\sigma}{1+\sigma^2}}$$

In summary, the conditions needed to have an asymptotic orbit with energy h are:

(a) the point (ξ_0, η_0, ζ_0) must be placed in the corridor defined by the Eqs. (10), (11) or (10), (12)

(b) the velocity must have the magnitude ρ expressed by (15), and the direction defined by the two angles θ and δ (according to (16)), with

$$\theta = \theta_{\min} \quad \text{or} \quad \theta = \theta_{\max} \quad \text{and} \quad \delta \in [\delta_{\min}, \delta_{\max}]$$

where $(\theta_{\min}, \theta_{\max})$ and $(\delta_{\min}, \delta_{\max})$are defined in (20) and (19), respectively.

On the other hand, if the angle θ is included in the interval $(\theta_{\min}, \theta_{\max})$ the constant α_1 is greater than zero, so the orbit is a transit orbit. Moreover, the values outside the interval correspond to $\alpha_1 < 0$ (bouncing orbits). Figure 4 represents the sphere of radius ρ of the admissible velocity vectors associated to a point (ξ_0, η_0, ζ_0) in the asymptotic corridor. If the tip of the velocity vector belongs to the interior of the region ABCD, then the orbit will be a transit orbit. If the tip of velocity lies along the boundary curve ABDC, then the orbit is an asymptotic orbit. Finally, if the tip is outside the region ABCD, then the orbit is a bouncing orbit.

The arcs AD, BC correspond to the difference $\Delta\delta = \delta_{\max} - \delta_{\min} = 2\delta_{\max}$, whereas the arcs AB, DC correspond to the difference $\Delta\theta = \theta_{\max} - \theta_{\min}$ at $\delta = \delta_{\max}, \delta = \delta_{\min}$, respectively. With reference to Fig. 3, let us consider the values $\xi_0 = -0.01$, $\zeta_0 = 0.001$ and η_0 equal to three distinct values along the vertical segment A_1A_2:

$$\eta_{01} = -0.0257\,, \quad \eta_{02} = -0.0110, \quad \eta_{03} = -0.0055$$

The planar projection (ξ_0, η_{01}) of the point $(\xi_0, \eta_{01}, \zeta_0)$, is on the boundary of the strip corresponding to $A_z = 0$, (that is $\delta = 0$, planar orbit), the projection (ξ_0, η_{03}) corresponds to the center of the strip, and the point (ξ_0, η_{02}) is mid-way between the above two points. The velocity locus related to the transit-asymptotic orbits associated to the three points $(\xi_0, \eta_{0i}, \zeta_0)\, i = 1, 3$ has the parameters reported in Table 1. Of course the region ABCD

Table 1 Parameters defining the velocity locus ABCD of transit-asymptotic orbits

η_0	ρ	$\theta_{\min}/\theta_{\max}(\delta = 0)$(deg)	$\theta_{\min}/\theta_{\max}(\delta = \delta_{\max})$(deg)	$\delta_{\min}/\delta_{\max}$(deg)
−0.0257	0.0199	24.71 / 24.71	24.71 / 24.71	0
−0.0110	0.0512	−31.48 / 80.91	−21.90 / 71.31	±35.92
−0.0055	0.0547	−29.86 / 79.28	−20.01 / 69.57	± 35.13

related to the point $(\xi_0, \eta_{01}, \zeta_0)$ collapses to a single point corresponding to the direction parallel to the strip that generates an asymptotic orbit.

Now points on the locus of asymptotic orbits will be propagated according to the nonlinear equations of motion (1).

Let us first consider planar cases: $\zeta_0 = w_0 = 0$. One hundred equally spaced values η_0 are taken along the segment $\xi_0 = -0.01$ inside the strip with energy $h = 0.001$. The positions (ξ_0, η_0) are propagated numerically by using the (nonlinear) planar restricted three-body model under the assumption of specified magnitude ρ for the velocity:

$$\rho^2 = 2h + a\xi_0^2 - b\eta_0^2$$

Nine different directions of the velocity are assumed for each point according to the following formula for the firing angle θ:

$$\theta = s\theta_{\min} + (1 - s)\theta_{\max}$$

where s is a parameter that varies in the interval [0, 1].

These 900 initial conditions are backward propagated up to the (first) perigee and propagated forward up to the (first) periselenium. It is worth remarking that all the orbits are transit orbits, as stated by the analysis of the linearized equations of motion. Figure 5 shows the (dimensionless) values of perigee and periselenium radii that can be reached starting from the 900 distinct initial conditions.

Figure 5 shows that, with the above fixed value of the energy h, the closest approach to the Earth occurs at about 75000 km of altitude, and the closest approach to the Moon is at an altitude of about 1000 km. These values are achieved by taking the velocity direction close to the minimum firing angle $\theta_{\min}$ ($s = 0.9$), which corresponds (in the linear approximation) to an asymptotic orbit. The same analysis is generalized to the three-dimensional case by adding the initial out-of-plane coordinate $\zeta_0 = 0.001$. Now the above three values η_{0i} are taken along the segment A_1A_2 of Fig. 3: the velocity magnitude is determined by the energy $h = 0.001$ and the velocity direction is defined by two parameters, s_1, s_2, according to the following relationships:

$$\delta = s_1\delta_{\min} + (1 - s_1)\delta_{\max}\,, \quad s_1 = 0.1, \ldots, 0.9$$
$$\theta = s_2\theta_{\min}(\delta) + (1 - s_2)\theta_{\max}(\delta)\,, \quad s_2 = 0.1, \ldots, 0.9$$

These initial conditions have been backward propagated up to the (first) perigee and propagated forward up to the (first) periselenium. It is worth remarking that all these three dimensional orbits are transit orbits, as stated by the analysis of the linearized equations of motion. Figures 6 and 7 show the (dimensionless) values of perigee and periselenium radii that can be reached starting from these initial conditions. Again lower perigee and periselenium values are achieved at the boundary of the region of (linear) transit orbits.

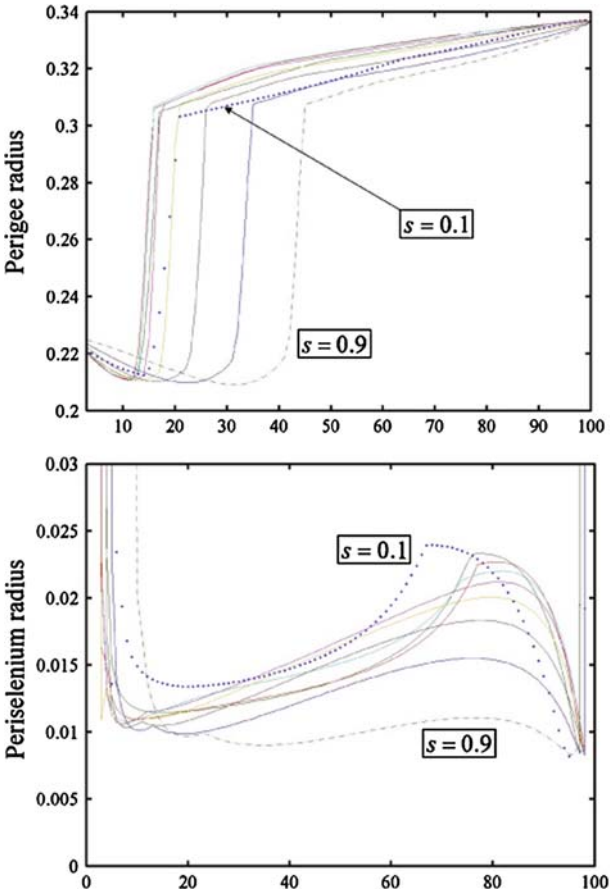

Fig. 5 Perigee and periselenium radii (in dimensionless units) obtained from one hundred points taken along the vertical segment ±35.13 (see Fig. 3), with nine different firing angles

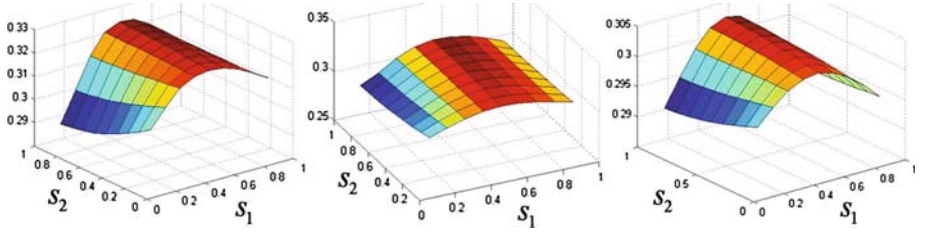

Fig. 6 Perigee radii (z-axis, DU) obtained after backward propagation from the points ±35.13, ±35.13, ±35.13, by employing 81 different firing angles

3 Targeting to the L1 region

3.1 Strategy

An Internal WSB transfer is generally composed of the following segments:

1. Launch
2. Near-Earth parking orbit apogee raising maneuver

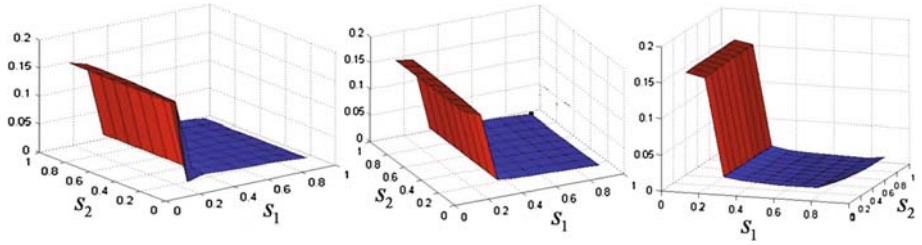

Fig. 7 Periselenium radii (z-axis, DU) obtained after forward propagation from the points ± 35.13, ± 35.13, ± 35.13, by employing 81 different firing angles

3. Bridge segment
4. Manifold insertion maneuver
5. Ballistic transfer trajectory (plus a course-correction maneuver if needed)
6. Ballistic lunar orbit insertion
7. Circularization maneuver (if required)

The main problem is determining point 5, i.e. finding a suitable WSB trajectory that meets the given mission requirements. The determination of all the other segments is then based upon this result. The first of two approaches that can be used when planning an Internal WSB lunar transfer is to choose a point along a LL1 quasi-periodic orbit as target. There are stable and unstable manifolds going to and departing from quasi-periodic orbits in the L1 region (Gomez et al. 2004, 2009; Koon et al. 1999): some properties of these manifolds in the vicinity of L1 have been discussed in Sect. 2. Among the stable manifolds, some run form the Earth region to L1 while others form the Moon to L1. Conversely, unstable manifolds can run from L1 either to the Earth region or to the Moon. With the correct energy, an Earth-to-L1 stable manifold can be connected with a L1-to-Moon unstable manifold, thus obtaining a transit orbit. The type of orbit (asymptotic or transit) is determined by the value of its Jacobi Constant. Since L1 is a connecting point for manifolds, quasi-periodic orbits are a sort of "gateway" to the Moon. It makes sense, then, to "target" a quasi-periodic orbit in order to find the desired WSB trajectory. A bridge segment is then needed because the internal stable and unstable manifolds do not cross low Earth orbits, since they approach the Earth at a minimum distance of about 65000 km. Thus, there is the need of connecting the low Earth orbit achieved after launch with the chosen SMD trajectory. The numerical procedure used is as follows:

1. Compute a L1 Lyapunov or quasi-periodic orbit using the linearized solution to the CR3BP, described in Sect. 2 (Fig. 8).
2. Select a point along the said orbit and extract its six-dimensional state vector (position and velocity components).
3. Initialize a backward-integration sequence inside STK/Astrogator with the state vector obtained in point 2. Run the sequence until the desired bridging point.
4. Retrieve the state vector at the bridging point and use it as target in a forward-integration sequence which starts from the post-launch parking orbit and performs the apogee raising maneuver needed to reach the selected manifold (bridge segment in Sect. 3.1). In this way, the correct launch time, launch azimuth and Delta-V can be computed.
5. Point 4 will take the spacecraft at the right place at the right time to intersect the WSB transfer trajectory, but not at the correct speed. One more targeting is required to compute the correct manifold insertion burn Delta-V.

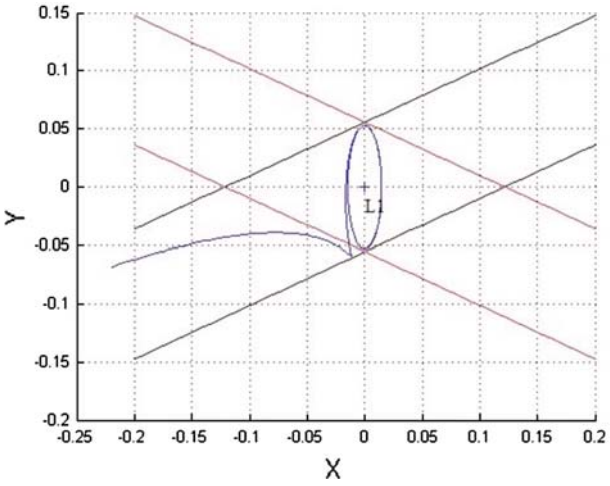

Fig. 8 A MATLAB plot of an asymptotic trajectory tending to a Lyapunov orbit around LL1, computed according to the linear model of Sect. 2. The axis show the value of the X and Y coordinates (DUs) of the Earth–Moon sinodic frame centered around L1

6. Propagating forward from the manifold insertion maneuver on should lead the spacecraft into a ballistic capture in a quasi-periodic orbit around LL1. In practice, as will be discussed below, most of times a small course-correction maneuver is required.
7. Once in the L1 region, there is still the need to forward-target a lunar ballistic capture orbit and, if required, a circularization maneuver.

The model considered for the integration of the equations of motion of the spacecraft includes the Earth, the Sun and the Moon, whose positions are taken from the JPL precise ephemerides DE405. Thus the trajectories found are in the non-circular and non-planar problem.

3.2 Results

It is interesting to note how solutions of the linearized model when backward-propagated with STK lead to nearly-asymptotic trajectories that are not too far from the linear solution. In most planar cases, they lead to ballistic captures in a Lyapunov orbit (Figs. 9, 10), while in most out-of-plane cases a small insertion Delta-V is needed. Getting to L1 by means of a WSB transfer is generally more economical than with a Hohmann transfer.

Once in the L1 region, we still need to target the desired lunar orbit. A course-correction Delta-V is needed at some point of the transfer to place the spacecraft in a trajectory that will transit through the L1 region leading to a ballistic capture around the Moon. The capture orbit must, at least, have the desired inclination and radius of periapse. The work of Parker (Parker 2007) shows that one of the most fuel efficient transfer-schemes is the so-called "open-point" transfer. Here, the bridging is done at the farthest approach point with the Earth of the backward-propagated transfer trajectory and the course-correction maneuver is performed soon thereafter. This is the strategy used for all the transfers treated in this section. Figure 9 shows an example of transfer leading to a Lyapunov orbit around LL1, while Fig. 10 gives a good idea of how closely the Lyapunov orbit achieved at the end of the integrated trajectory matches the linearized "target" orbit.

The simulations show that there is no significant difference in terms of Delta-V between a ballistic capture into a Lyapunov orbit around L1 and a ballistic capture into lunar orbit. The total Delta-V does not usually exceed 3.9 km/s, with over 99% of the entire budget delivered

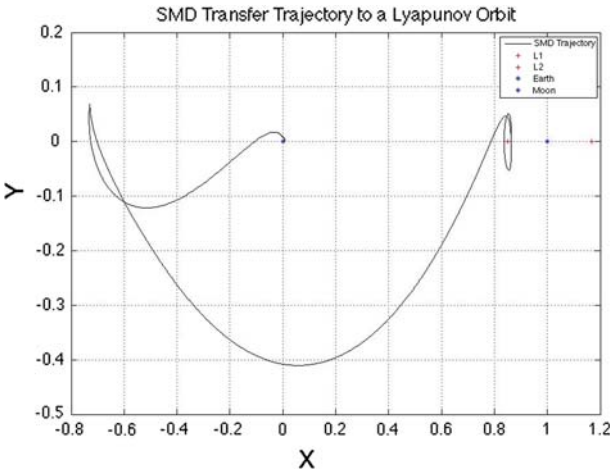

Fig. 9 The complete transfer from a low Earth orbit to a Lyapunov orbit around LL1 described in Sect. 3.2, Table 2. It can be seen that the orbit leads to a Lyapunov orbit of amplitudes very close to those of Fig. 8. The axis show the value of the X and Y coordinates (DUs) of the Earth–Moon sinodic frame centered around the Earth

Table 2 Summary of the Delta-V required for the transfer to the Lyapunov orbit shown in Fig. 9

Segment	Delta-V (km/s)
Raising apoapsis	2.96
Manifold injection burn	0.88
Course-correction burn	0.012
Orbit injection	0
Total	3.852
Transfer time (days)	20

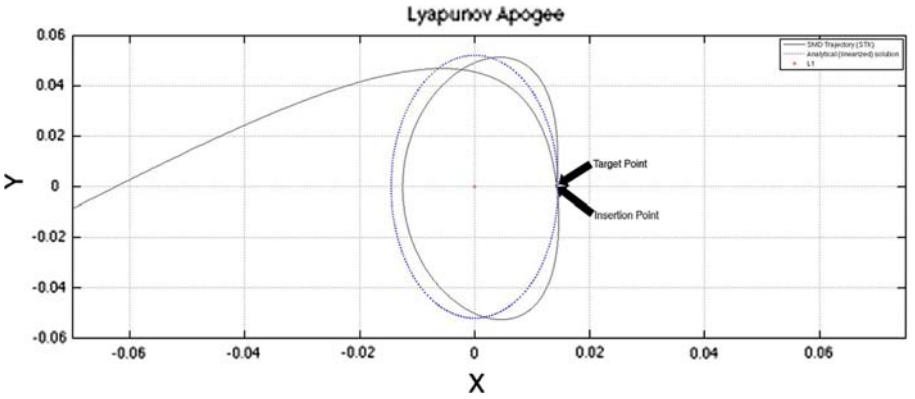

Fig. 10 This figure shows a comparison between the linearized Lyapunov orbit used to compute the target point (*blue dashed line*) and the Lypaunov orbit achieved after numerical integration in the 4-body problem (*black continuous line*). It is worth noting that the target point and insertion point do not differ more than 100 km along the X axis. The axis show the value of the X and Y coordinates (DUs) of the Earth–Moon sinodic frame centered around L1

by the launcher (under the assumption that the manifold insertion maneuver is performed by a restartable fourth stage).

What raises the cost of a lunar mission is usually the need to circularize the orbit, and the lower is the desired radius the higher is the cost. From a 10000 km radius down to a 100 km radius orbit, the Delta-V required for circularization ranges from about 150 m/s to about 600 m/s. The Delta-V percentage delivered by the launcher drops to about 93% and 86%, respectively, thus raising accordingly the percentages to be provided by the spacecraft. If we look at the total Delta-V, this kind of transfer does not perform well when the target is a low lunar orbit, equaling, at best, a Hohmann transfer (Perozzi and DiSalvo 2008). This is partly inherent in this type of transfer and partly due to the fact that targeting from L1 to the Moon is not easy and usually the capture orbit obtained has an eccentricity (above 0.9) higher than the value predicted theoretically.

However, it must be noted that:

(a) The capture into lunar orbit requires no Delta-V, and, although unstable, guarantees at least a week before escape for very high eccentricity values (Winter and Vieira 2002; de Melo et al. 2007). Hence, there is no need for a large impulsive maneuver, but the orbit can be circularized more slowly, for example by means of an electrical engine.
(b) Since a ballistic capture orbit has an eccentricity that is, by definition, always less then 1, the Delta-V that the spacecraft must provide to achieve a circular orbit is always less than the corresponding Delta-V in the Hohmann transfer case. This translates into saving up to about 200 m/s when comparing to a classical LOI maneuver

In conclusion, this means that using this kind of transfer results in a different distribution of the Delta-V between launcher and spacecraft rather then a net decrease. This means a larger spacecraft dry mass, which in turn may allow the use of a spacecraft bus otherwise not fitting the propulsion requirements (e.g. fuel capacity) of a classical lunar transfer. However this is achieved at the cost of a longer transfer time (10–15 days longer than Hohmann).

4 Direct targeting to a lunar capture orbit

4.1 Theory

Let us define the concept of Weak Stability Boundary region around the Moon, in the restricted three body problem. When restraining to two-body motion, a spacecraft traces the same orbit around the Moon indefinitely, no matter its radius, provided that the velocity is less then the escape velocity. The WSB is a region of phase-space where each point (defined by both position and velocity) is such that any body with negligible mass (i.e. the spacecraft) will not remain bounded to the Moon indefinitely. Instead, it will escape after a finite number of revolutions and end up into an orbit around the Earth. Note that in this case, the velocity in the WSB is always less than the escape velocity. This process is often referred to as "ballistic escape". Conversely, if a spacecraft approaches the Moon with a state (in phase-space) that is inside the WSB, it will be captured without the need for a maneuver into a highly elliptical orbit for a finite period of time.

According to Belbruno (Belbruno 2004), the WSB region can be defined mathematically in a three-dimensional sinodic frame as the region in which Eq. (21) is satisfied.

$$C = -r\left(\pm 2\sqrt{\frac{\mu\,(1+e)}{r}} + r\right) + \frac{\mu\,(1-e)}{r} + A\,(r,\theta,\varphi) \tag{21}$$

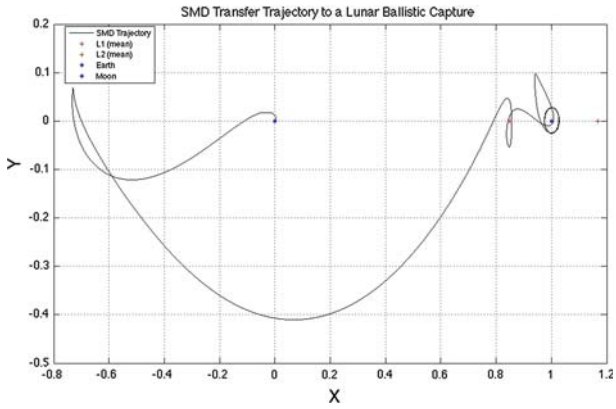

Fig. 11 With a small variation of the mission profile of Fig. 9 (about 1 m/s), a lunar ballistic capture orbit can be obtained

where

$$A\,(r,\theta,\varphi) = (r_x - 1 + \mu)^2 + r_y^2 + r_z^2 + 2\frac{(1-\mu)}{r_t} \tag{22}$$

Writing explicitly the radius vector components r_x, r_y, r_z in Eqs. (21) and (22), yields:

$$C = -r\left(\pm 2\sqrt{\frac{\mu\,(1+e)}{r}} + r\right) + \frac{\mu\,(1-e)}{r} + (r\cos\theta\cos\varphi - 1 + \mu)^2 + (r\sin\theta\cos\varphi)^2 + (r\sin\varphi)^2 - 2\frac{(1-\mu)}{r_t} \tag{23}$$

where r is the radius from the current attracting body (e.g. the Moon), r_t is the radius from the third body (e.g. the Earth), θ is the in-plane angle from the X axis, ϕ is the angle between the XY plane and the radial vector, and the other variables follow the same notation as in Sect. 2. The $\pm$ sign differentiates Internal and External transfers, respectively.

Solving the equation above for e gives, for a fixed Jacobi constant, the eccentricity that an orbit must have at any given distance form the Moon to lie inside the WSB region. If we are targeting a lunar encounter at periselenium (very common in mission design), the velocity associated to a given value of the periselenium that guarantees ballistic capture follows directly from the eccentricity (Fig. 11).

$$v_p = \sqrt{\frac{GM_{\text{moon}}\left(\frac{2}{1-e} - 1\right)}{\frac{r_p}{1-e}}} \tag{24}$$

Where GM_{moon} denotes the dimensional Moon mass parameter

Note from Fig. 12 the high values of the eccentricity involved in a low altitude (100 km) periselenium of the capture orbit. The relatively large magnitude of the circularization maneuver needed to reach a circular low altitude operational orbit as typical of most remote sensing missions, reduces the advantage achieved through ballistic capture, in terms of overall delta-V. However, electric propulsion for reaching a low altitude circular orbit can be applied more effectively if the spacecraft undergoes a gravity capture. It is also interesting to note how ballistic capture opens up new possibilities. For instance, the capture orbit could be modified through Earth gravity assists (an example of this is shown in Fig. 13).

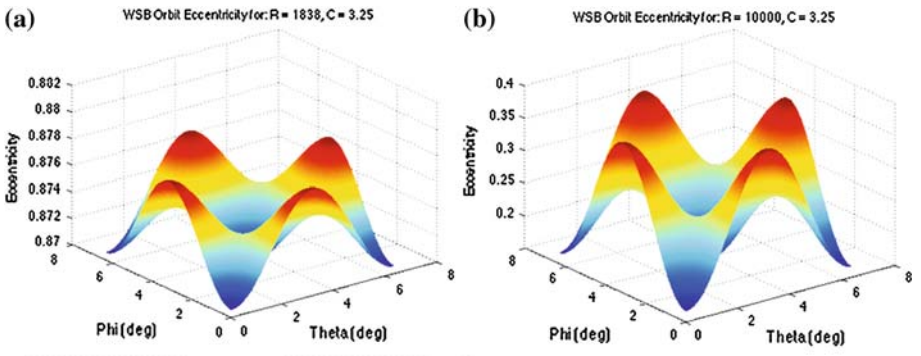

Fig. 12 **a** The eccentricity associated to a lunar WSB capture orbit for a fixed Jacobi Constant $C = 3.2$ and a fixed periselenium radius of 1838 km. The figure shows how the e_{WSB} changes with θ and ϕ (respectively, the longitude starting from the Earth–Moon line and the elevation above the Moon equator); **b** The same plot as in (**a**) but with a periselenium radius fixed at 10000 km

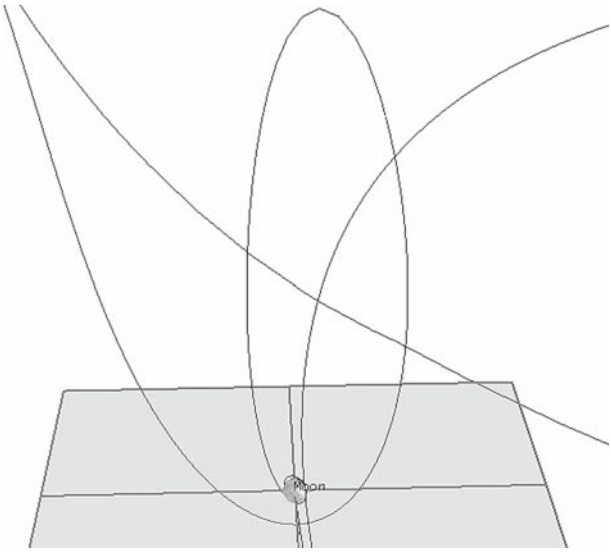

Fig. 13 The ballistic capture orbit achieved by targeting the lunar WSB region as described in Sect. 4.3, Table 4

4.2 Strategy

The WSB transfer in this case is still composed of the same building blocks as in Sect. 3.1. The difference is that instead of targeting a point in the L1 region using the equations developed in Sect. 2, the target will be a ballistic capture orbit around the Moon, computed through Eq. (23). This method is convenient because the targeting is done directly to the final orbit and avoids the need for a second targeting from L1 to the Moon. As it will be shown, the trajectory does not transit through a quasi-periodic orbit and, thus, this method can only be used for planning lunar transfers. The procedure, very similar to the one outlined in Sect. 3, is as follows:

1. By means of Eqs. (23), (24), find a lunar orbit which is inside the WSB region around the Moon and has the desired periapse radius and inclination.

Table 3 Summary of the Delta-V required for achieving a 10000 km circular lunar orbit shown in Fig. 11

Segment	Delta-V (km/s)
Raising apoapsis	2.96
Manifold injection burn	0.88
Course-correction burn	0.013
Lunar orbit injection	0 ($e = 0.9$)
Circularization	0.180
Total	4.032
Transfer time (days)	30

2. Initialize a backward-integration sequence inside STK/Astrogator with the orbital elements obtained in point 1. Run the sequence until the desired bridging point is achieved.
3. Retrieve the state vector at the bridging point and use it as target in a forward-integration sequence within STK/Astrogator. In this way, the correct launch time, launch azimuth and Delta-V value for the "raising apogee" maneuver can be computed.[1]
4. Point 3 brings the spacecraft at the right place at the right time to intersect the Internal WSB transfer trajectory, but not at the correct speed. One more targeting is required to compute the correct "manifold insertion burn" Delta-V.
5. Propagating forward from this point on leads the spacecraft into a ballistic capture around the Moon.

4.3 Results

As in Sect. 3.2, the forces considered for the integration of the spacecraft equations of motion are that of the Earth, the Sun and the Moon. The positions of the celestial bodies are determined through the JPL precise ephemerides database DE405. Therefore, the resulting trajectories are non-circular and non-planar.

As it can be seen from Tables 3, 4 and 5, this method leads to more efficient transfers to lunar orbits than those obtained in Sect. 3. The difference in terms of total Delta-V, for the same target orbit, is as high as 300 m/s. In the case of a 100 km polar orbit (Fig. 13), the total Delta-V is very similar to that of a Hohmann transfer. However, it can be seen from Table 4 that the Delta-V that must be supplied by the spacecraft is as low as 595 m/s, with a net decrease of 205 m/s with respect to Hohmann. It can also be seen that the ballistic capture orbit has a lower eccentricity then that shown in Table 3. Moreover, the eccentricities obtained both for a capture orbit with a 100 km radius and for a 10000 km one, are in the range predicted by the theory and shown in Fig. 12a and b.

[1] This problem can be summarized as follows. Since STK uses actual ephemerides for computing the position of Earth, Sun and Moon it needs to know the epoch at which the spacecraft trajectory shall be calculated (e.g. the launch date and time). Furthermore, the "manifold insertion" maneuver Delta-V given by the linearized model can only be considered a "first guess" because of the differences, however small, introduced by the presence of a fourth attracting body and the non-circularity of the problem. Thus, there are three unknown quantities in the problem that need to be calculated: two launch conditions (epoch and azimuth) and the maneuver Delta-V. STK/Astrogator differential corrector uses an iterative process to numerically correct the "first guess" solutions and find the needed quantities. See Appendix A for a brief explanation of the method.

Table 4 Summary of the Delta-V required for the transfer to a lunar orbit targeting the lunar WSB region

Note that the final lunar orbit here is much lower than that in the previous section and has a radius of 100 km ($i = 90°$)

Segment	Delta-V (km/s)
Raising apoapsis	2.83
Manifold injection burn	0.71
Course-correction burn	0
Lunar orbit injection	0 ($e = 0.8$)
Circularization	0.595
Total	4.135
Transfer time (days)	19

Table 5 Summary of the Delta-V required for a transfer to a lunar orbit that has the same target conditions as in the transfers shown in Fig. 11, namely a 10000 km circular orbit

It can be seen how this transfer performs significantly better

Segment	Delta-V (km/s)
Raising apoapsis	2.83
Manifold injection burn	0.74
Course-correction burn	0
Lunar orbit injection	0 ($e \sim 0.5$)
Circularization	0.200
Total	3.77
Transfer time (days)	19

5 Deploying a three-satellite constellation

5.1 Overview

This section briefly presents the results obtained form a simulation of a WSB transfer for multiple spacecraft. The goal of this study is to prove that it is possible to launch more than one spacecraft onboard a single launch vehicle, place them initially in the same WSB transfer trajectory, and exploit its chaotic nature for driving them to significantly different lunar orbits (i.e. with little fuel consumption),.

The main purpose of the constellation is to provide a telecommunications link between the Earth and the whole lunar surface,. It has been known since the 1960s that a continuous link with the far side of the Moon can be achieved with just one relay spacecraft in a halo or Lissajous orbit around the Earth–Moon L2 point (Farquhar 1967). However, the multiple satellite approach has been chosen here for two main reasons: while it is true that a single L2 satellite provides full coverage of the far side, it cannot act as a relay for transmitters located in the near side. This implies that a transmitter in the near side should have enough EIRP to provide a good direct link with Earth. This is not always the case, particularly for small rovers. The constellation approach enables a high data rates link with every site on the lunar surface even with a rover equipped with a patch antenna with a gain no greater than 6 db. Secondly, a telecom constellation can be used for navigation purposes as well, thus providing two key services with the same asset.

The design of the transfer trajectory adopted for delivering the three-satellite constellation described in what follows was originally developed with the targeting-to-L1 approach

Table 6 Summary of the Delta-V required for the first part of the transfer, common to all three satellites, provided by the launcher

Segment	Delta-V (km/s)
Common transfer lag	
Raising apoapsis	297
Manifold injection burn	0.84
Total	3.81

Table 7 Summary of the Delta-V required for the first Satellite to complete its transfer

Segment	Delta-V (km/s)
Satellite 1 after separation	
Course-correction burn	0.055
Lunar orbit injection	0
Circularization	0.180
Total	0.235
Transfer time (days)	26
Satellite 1 orbital parameters at first periselenium	
R_p (km)	10000
e	∼0.67
i (°)	70
Arg. of periselenium (°)	34.82
Longitude of asc. Node (°)	103.78

Table 8 Summary of the Delta-V required for the second Satellite to complete its transfer

Segment	Delta-V (km/s)
Satellite 2 after separation	
Course-correction burn	0.032
Lunar orbit injection	0
Circularization	0.183
Total	0.215
Transfer time (days)	21
Satellite 2 orbital parameters at first periselenium	
R_p (km)	10000
e	∼0.69
i (°)	70
Arg. of periselenium (°)	307.55
Longitude of asc. Node (°)	307.8

described in Sect. 3. The effects of the Earth, Sun and Moon gravity are considered and their motion is modeled after the JPL DE405 ephemerides.

Table 9 Summary of the Delta-V required for the third Satellite to complete its transfer

Segment	Delta-V (km/s)
Satellite 3 after separation	
Course-correction burn #1	0.028
Course-correction burn #2	0.042
Lunar orbit injection	0
Circularization	0.158
Total	0.228
Transfer time (days)	28
Satellite 3 orbital parameters at first periselenium	
R_p (km)	10000
e	~0.3
i (°)	70
Arg. of periselenium (°)	97.27
Longitude of asc. Node (°)	39.1

5.2 Results

The results obtained are summarized in Tables 6,7,8 and 9. Under the assumption that the launch vehicle releases the three satellites together after the manifold insertion burn, about 94% of the total Delta-V (4 km/s) necessary for the transfer is delivered by the launcher itself. Only the remaining 6%, little more than 200 m/s, is at the expense of the single satellite. Furthermore, about 4.5% of the budget is spent for the circularization maneuver only. In this respect the longer time allowed to reach the desired operational orbit by the ballistic capture, can bring further advantages if the spacecraft is equipped with a low-thrust engine which provides more efficiently the required orbital change. Hence, there is only the need to equip the spacecraft with a propulsion system capable of delivering, in a single maneuver, a maximum of 60 m/s. This scenario supports the conclusion that launching multiple lunar satellites using a WSB transfer is not only feasible but it also allows major savings on the spacecraft masses.

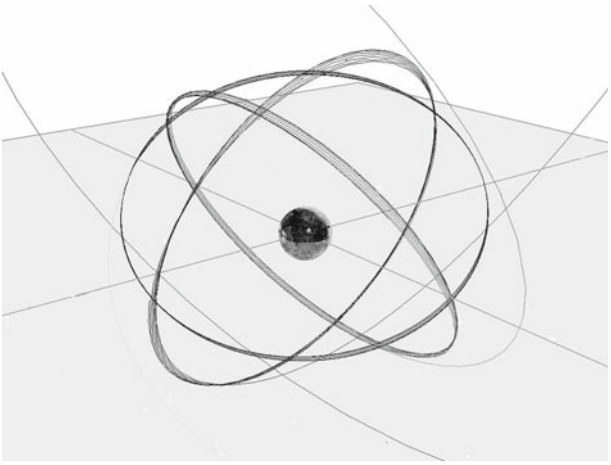

Fig. 14 The constellation achieved after transfer is complete for all three satellites

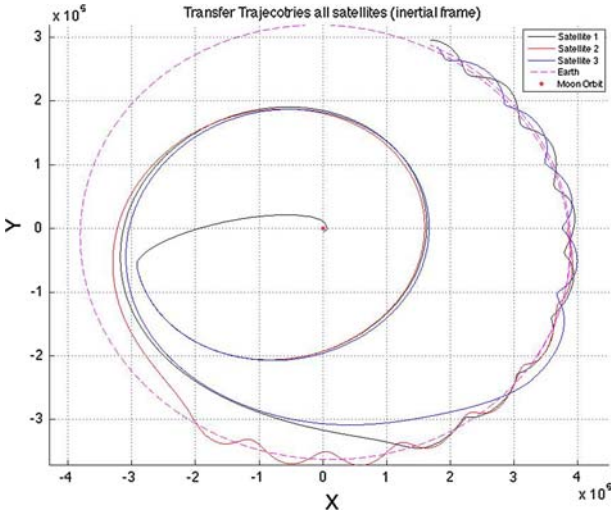

Fig. 15 The complete transfer for all three spacecraft shown in the Earth-centered inertial reference frame

Figure 14 shows the final constellation after circular orbits are achieved, while trajectories for all satellites in the inertial frame are shown in Fig. 15.

6 Conclusions

The concepts of Space Manifold Dynamics and Week Stability Boundary are relatively new in space mission design, yet they have proven to provide an efficient alternative option to classical mission design. Several applications have been carried out for reaching halo orbits around the Earth–Sun Lagrangian point EL_1(e.g. the ESA SOHO mission), while most of the future astronomical observatories in space are aimed to the Earth–Sun Lagrangian point EL_2. As far as the Moon is concerned, to date there have been two attempts of using SMD transfers: by the European SMART-1 mission and by the Japanese Hiten spacecraft which successfully achieved the first ballistic capture around the Moon in 1991. As far as modeling SMD transfers is concerned, most of the literature involve studies made under simplifying assumptions like the CR3BP. Moreover no commercial software has so far implemented methods specifically devoted to routinely perform SMD mission design.

In our study proof has been given that linearized (or otherwise simplified) analytical solutions of the three-body problem can be effectively used in conjunction with a commercial software (STK). Indeed, it has been shown that the search algorithms within STK converge to a SMD solution even when fourth-body or other perturbations are accounted for in the model. The method presented here provides a means of handling these new techniques in mission design inside an existing (and certified) software framework. In Tables 10 and 11 the simulations carried out in Sects. 3 and 4 are summarized, showing that the numerical results agree with the theory outlined in Sects. 2 and 4. Ballistic capture orbits with increasingly higher periselenium have lower eccentricities and, thus, the circularization maneuver has a magnitude inversely proportional to the periselenium distance.

Note that although periodic or quasi periodic internal transfers can be found which allow extra savings in ΔV with respect to the values reported in Tables 10 and 11, the corresponding increase of the transfer times makes them less appealing for practical applications, especially

Table 10 Comparison of the results obtained for the same transfer (LEO parking orbit to a 100 km lunar circular polar orbit) using the techniques described in Sects. 3 and 4

Segment	Direct lunar targeting SMD transfer ΔV (km/s)	Lunar SMD transfer through L1 ΔV (km/s)
Raising apoapsis	2.83	2.97
Manifold injection burn	0.71	0.84
Course-correction burn	0.00	0.07
Lunar orbit injection	($e = 0.8$) 0.00	($e = 0.94$) 0.00
Circularization	0.60	0.65
Total	4.14	4.53
Transfer time (days)	19	30

Table 11 Comparison of the results obtained for the same transfer (LEO parking orbit to a 10000 km lunar circular orbit) using the techniques described in Sects. 3 and 4

Segment	Direct lunar targeting SMD transfer ΔV (km/s)	Lunar SMD transfer through L1 ΔV (km/s)
Raising apoapsis	2.83	2.97
Manifold injection burn	0.74	0.84
Course-correction burn	0.00	0.06
Lunar orbit injection	($e \sim 0.5$) 0.00	($e = 0.67$) 0.00
Circularization	0.20	0.18
Total	3.77	4.05
Transfer time (days)	19	30

as far as manned missions are concerned (Compagnone and Perozzi 2007; Topputo et al. 2005).

Thus, some general conclusions on the use of internal WSB transfers to the Moon can be drawn:

1. small changes in the choice of the incoming transfer trajectory lead, through ballistic capture, to widely different orbits around the Moon (e.g. from equatorial to polar);
2. high-eccentricity or high-altitude operational orbits around the Moon strongly decrease the magnitude of the total ΔV because they avoid performing circularization maneuvers deep inside the gravity well of the Moon;
3. generally lower values of the total ΔV budget, of the eccentricity of the capture orbit and of the transfer time are obtained when the direct lunar targeting is adopted instead of entering the lunar sphere of influence through L_1 (see Tables 10, 11).

These considerations have been used as drivers for carrying out a comprehensive simulation on the place-in-orbit of a three-satellite constellation around the Moon. In an extensive lunar exploration scenario multi-spacecraft missions of this kind are expected to guarantee telecommunications with the Earth from the lunar far side and can be employed also for navigation purposes. It is shown that the nominal orbital configuration of the lunar constellation is obtained by launching all satellites at the same time into a high eccentricity near-Earth orbit for performing a common manifold insertion maneuver. The three spacecraft are then

separated from the launcher and provide by their own means the ΔV required to achieve different ballistic capture orbits around the Moon.

Acknowledgments The authors would like to thank the SpaceOPS Academy for having provided the occasions for fruitful discussions and confrontations on the subject of this paper. R.M. acknowledges the support of Telespazio LSS (Laboratorio di Simulazione di Sistemi) and wishes to thank Francesco Mazzuca, Walter Pecorella and Giuseppe Corrao.

Appendix A

STK/Astrogator differential corrector (STK Help 2008)

The problem that the differential corrector needs to solve is finding the values of some unknown (independent) variables that meet a given set of orbital goals. The goal G(v) is expressed in terms of a pseudo-Taylor series expansion of the independent variable v, typically truncated at the first order. In the case of a single-dimension problem:

$$G_1(v_1) \approx G_0 + \frac{dG}{dv}(v_1 - v_0)$$

Thus, the value v_1 can be expressed as:

$$G_1' = \frac{dG}{dv} \approx \frac{G_1 - G_0}{v_1 - v_0}$$
$$v_1 \approx v_0 + \frac{G_T - G_0}{G_1'} = v_0 + (G_T - G_0)\left[G_1'\right]^{-1}$$

where v_1 represents the approximated value of the independent variable needed to meet the goal G_T if the initial value $v_0$is known and an approximation of the derivative G_1'can be found. In the case presented in this paper, the variables $v_1^i$are the launch epoch, launch azimuth and maneuver Delta-V magnitude, whereas the goals are represented by the orbital parameters of the lunar orbit achieved after ballistic capture. To generate the approximation of the values $v_1^i$the algorithm perturbs each variable $v_0^i$by a small amount δv_i and measures the resulting change in each goal. It then integrates a nominal trajectory and uses the results to calculate an approximation of the derivative $G_1^{j\prime}$and a new estimate of the variables v_0^i. This process is then repeated until the achieved value of the goal falls within the (user-specified) tolerance for the goal. Starting values for the independent variables that are not too far from the actual solution are needed for the process to converge. In our case, these "first guess" values are computed through the analytical model.

References

Baig, S., McInnes C.R.: Artificial halo orbits for low-thrust propulsion spacecraft. Celest. Mech. Dyn. Astron. **104**(4), 321–335 (2009)

Barrabés, E., Mondelo, J.M., Ollé, M.: Dynamical aspects of multi-round horseshoe-shaped homoclinic orbits in the RTBP. Celest. Mech. Dyn. Astron. **105**(1–3), 197–210 (2009)

Belbruno, E.: Capture Dynamics and Chaotic Motions in Celestial Mechanics. Princeton University Press, Princeton (2004)

Circi, C., Teofilatto, P.: WSB trajectories for the deployment of lunar spacecraft constellations. Celest. Mech. Dyn. Astron. **95**, 371–390 (2006)

Compagnone, F., Perozzi, E. (eds.): Moon Base: A Challenge for Humanity. Donzelli Editore, Roma (2007)

Conley, C.: Low energy transit orbits in the restricted three body problem. SIAM J. Appl. Math. **16**, 732–746 (1968)
de Melo, C.F., et al.: Numerical Study about Natural Escape and Capture Routes by the Moon via Lagrangian Points L1 and L2. Adv. Space Res. **40**(1), 83–95 (2007)
Érdi, B., Forgács-Dajka, E., Nagy, I., Rajnai, R.: A parametric study of stability and resonances around L4 in the elliptic restricted three-body problem. Celest. Mech. Dyn. Astron. **104**(1–2), 145–158 (2009)
Farquhar, R.W.: Lunar communications with libration point satellites. J. Spacecr. Rockets **4**, 1383–1384 (1967)
Garcia, F., Gomez, G.: A note on weak stability boundaries. Celest. Mech. Dyn. Astron. **97**, 87–100 (2007)
Gomez, G., Koon, W.S., Lo, M.W., Masdemont, J.E., Ross, S.D.: Connecting Orbits and Invariant Manifolds in the Spatial Restricted Three Body Problem, Nonlinearity No. 17, pp. 1571–1606. Institute of Physics Publishing (2004)
Gomez, G., Masdemont, J.J., Mondelo, J.J.: Invariant manifolds for space mission design. Computational aspects. In: Perozzi, E., Ferraz-Mello, S. (eds.) Space Manifold Dynamics. Springer, New York (2009)
Koon, W.S., Lo, M.W., Marsden, J.E., Ross, S.D.: Dynamical Systems, the Three-Body Problem and Space Mission Design. Proceedings—International Conference on Differential Equations, Berlin (1999)
Leiva, A.M., Briozzo, C.B.: Extension of fast periodic transfer orbits from the Earth–Moon RTBP to the Sun–Earth–Moon quasi-bicircular problem. Celest. Mech. Dyn. Astron. **101**(3), 225–245 (2008)
Moeckel, R.: A variational prrof of existence of transit orbits in the restricted three body problem. Dyn. Syst. **20**, 45–58 (2005)
Mingotti, G., Topputo, F., Bernelli-Zazzera, F.: Low-energy, low-thrust transfers to the Moon. Celest. Mech. Dyn. Astron. **105**(1–3), 61–74 (2009)
NASA Exploration Systems Architecture Study, Final report, NASA-TM-2005- 214062. (2005)
Parker, J.S.: Low Energy Ballistic Lunar Transfers. Ph.D. Thesis, Department of Aerospace Engineering Sciences, University of Colorado at Boulder (2007)
Pergola, P., Geurts, K., Casaregola, C., Andrenucci, M.: Earth–Mars halo to halo low thrust manifold transfers. Celest. Mech. Dyn. Astron. **105**(1–3), 19–32 (2009)
Perozzi E., Ferraz-Mello S. (eds.): Space Manifold Dynamics, Springer US (2009) (in press)
Perozzi, E., DiSalvo, A.: Novel spaceways for reaching the moon: an assessment for exploration. Celest. Mech. Dyn. Astron. **102**, 207–218 (2008)
STK online help, Analysis Modules/Astrogator/Technical Notes, Differential Corrector (STK v8.1.3, 2008)
Szebehely, V.: Theory of Orbits. The restricted problems of three bodies. Academic Press, New York (1967)
Topputo, F., Vasile, M., Bernelli-Zazzera, F.: Earth-to-Moon low energy transfers targeting L1 hyperbolic transit orbits. Ann. N. Y. Acad. Sci. **1065**, 55–76 (2005)
Winter, O.C., Vieira Neto, E.: Distant stable orbits around the Moon. Astron. Astrophys. **393**, 661–671 (2002)